HHS Public Access

Author manuscript

HPB (Oxford). Author manuscript; available in PMC 2020 October 01.

Published in final edited form as:

HPB (Oxford). 2019 October ; 21(10): 1344–1353. doi:10.1016/j.hpb.2019.01.019.

Normal and Fibrotic Liver Parenchyma Respond Differently to Irreversible Electroporation

Chenang Lyu[a], **Maya Lopez-Ichikawa**[b], **Boris Rubinsky**[a], **Tammy T. Chang**[b]

[a]Department of Mechanical Engineering, University of California, Berkeley, CA 94720

[b]Department of Surgery, University of California, San Francisco, CA 94143

Abstract

Background: The safety and efficacy of irreversible electroporation (IRE) in treating hepatic, biliary, and pancreatic malignancies are active areas of clinical investigation. In addition, recent studies have shown that IRE may enable regenerative surgery and *in vivo* tissue engineering. To use IRE effectively in these clinical applications, it is important to understand how different tissue microenvironments impact the response to IRE. In this study, we characterize the electrical and histological properties of non-fibrotic and fibrotic liver parenchyma before and after IRE treatment.

Methods: Electrical resistivity and histology of fibrotic liver from C57BL/6 mice fed a 0.1% 3,5-diethylcarbonyl-1,4-dihydrocollidine (DDC) diet were compared to those of non-fibrotic liver from matched control mice before and after IRE treatment.

Results: At baseline, the electrical resistivity of fibrotic liver was lower than that of non-fibrotic liver. Post-IRE, resistivity of non-fibrotic liver declined and then recovered back to baseline with time, correlating with hepatocyte repopulation of the ablated parenchyma without deposition of fibrotic scar. In contrast, resistivity of fibrotic liver remained depressed after IRE treatment, correlating with persistent inflammation.

Discussion: Non-fibrotic and fibrotic liver respond to IRE differently. The underlying tissue microenvironment is an important modifying factor to consider when designing IRE protocols for tissue ablation.

Introduction

Irreversible electroporation (IRE) is a tissue ablation technology that employs short, high electric field pulses to permanently permeabilize cells and induce cell death.[1] A unique feature of IRE is that it induces cell death within tissues while leaving the extracellular

Corresponding author: Tammy T. Chang, MD, PhD, 513 Parnassus Ave., HSW1607, San Francisco, CA 94143, tammy.chang@ucsf.edu.

This work was presented as an oral presentation at the 2018 Americas Hepato-Pancreato-Biliary Association (AHPBA) Annual Meeting, March 7-11, 2018, Miami Beach, FL.

matrix intact, allowing repair of the ablated tissue without formation of scar.[2-6] Although some studies suggest that IRE induces cell death by apoptosis,[7-9] recent data show that IRE induces more immunogenic forms of cell death, including pyroptosis and necroptosis.[10] Immunogenic effects of IRE are evidenced by its ability to induce tumor regression at sites distant from the treated target tissue.[11] Determining the role of IRE in the treatment of hepatic, biliary, and pancreatic malignancies is an active area of clinical investigation,[12-21] and IRE may potentially be combined with immunotherapy to treat advanced cancers.[22,23]

In addition to clinical applications in tumor ablation, IRE may be an enabling technology for tissue engineering and regenerative surgery. IRE kills cells without destroying the extracellular matrix, thereby producing decellularized scaffolds that can be reseeded with new cells.[24-26] Moreover, IRE treatment of host liver parenchyma creates a niche that is supportive of *in vivo* engraftment of exogenously implanted hepatocytes.[27] These results suggest that IRE may be developed to facilitate engraftment of stem-cell-derived cells into dysfunctional solid organs, constituting a minimally-invasive form of regenerative surgery that can be an alternative or adjunct to transplantation as a treatment for end-stage organ failure.

Both tumor ablation and regenerative surgery applications require knowledge of how IRE may affect fibrotic tissues differently than non-fibrotic tissues, and this knowledge is currently lacking. Fibrotic tissues are characterized by a stiffened extracellular matrix, deposition of aligned collagen fibers, and chronic infiltration of inflammatory cells. These factors may alter the conductivity of the tissue.[28] In addition, due to differing cell sizes and morphologies, infiltrating immune cells and activated myofibroblasts may respond differently to IRE pulses than parenchymal cells.[29-32] For liver tumors, IRE is most commonly being used to treat colorectal metastases, which generally occur in non-fibrotic livers, and hepatocellular carcinomas, which occur more frequently in fibrotic livers.[16-19,33,34] Therefore, it is possible that the optimal IRE regimens to treat liver colorectal metastases versus hepatocellular carcinoma may be different because of differences in the underlying tissue milieu. In addition, end-stage organ failure, and in particular end-stage liver disease, typically present in adults in the setting of advanced tissue fibrosis.[35] Thus, it is also critical to determine the factors that regulate the response of fibrotic tissues to IRE in order to develop the technology for regenerative surgery purposes.

Electrical resistance is the measure of how much a material opposes the flow of current. Resistance (R), measured in units of ohms (Ω), is defined by Ohm's law as the ratio of voltage (V) to current (I) within a circuit, R=V/I. Whereas resistance is modulated by a material's length and cross-sectional area, resistivity is represented in units of ohms-cm (Ω·cm) and describes the intrinsic property of the material to oppose the flow of current. Impedance (Z) extends the concept of resistance in direct current circuits to alternating current circuits and is useful in assessing the response of tissues to IRE treatment. IRE induces formation of permanent nanopores within cell membranes, resulting in characteristic decrease in tissue impedance after treatment.[36] While mechanisms regulating changes in tissue impedance are complex and likely multi-factorial, measuring impedance has been proposed as a way to determine the extent of IRE-mediated tissue ablation.[36-38]

We hypothesized that intrinsic resistivities of non-fibrotic versus fibrotic tissues are different, and that fibrotic tissues respond to IRE differently and would exhibit distinct impedance profiles post-IRE compared to non-fibrotic tissues. To test these hypotheses, we determined the *in vivo* resistivity and/or impedance of non-fibrotic and fibrotic livers of mice before and after IRE treatment and correlated the electrical properties of the tissues with histological findings. The overall goal was to advance our understanding of how tissue microenvironments modulate cellular responses to IRE and to inform the design of IRE regimens for clinical applications such as tumor ablation and regenerative surgery.

Methods

Mice.

Male 6-8 week-old C57BL/6 mice were purchased from Jackson Laboratory (Bar Harbor, ME). All mice were cared for in accordance to the National Institutes of Health "Guide for the Care and Use of Laboratory Animals." Only male mice were used in these experiments because male and female mice develop different disease phenotypes in response to 3,5-diethoxycarbonyl-1,4-dihydrocollidine (DDC) intoxication.[39] Our experimental goals were to determine the differences in electrical properties between control non-fibrotic and fibrotic liver; therefore, it was desirable to minimize variability within the fibrosis group.

Experimental Liver Fibrosis.

Mice were given a standard mouse chow diet supplemented with 0.1% DDC (Sigma-Aldrich, St. Louis, MO) for 4 weeks to induce cholestatic liver fibrosis.[40] Control mice were maintained on standard mouse chow diet for comparison.

IRE.

Anesthesia, aseptic technique, perioperative care, and analgesia were performed in accordance to standard procedures and protocols approved by the Institutional Animal Care and Use Committee at UCSF. To expose the liver, a 1-cm incision along the midline was made directly below the xiphoid. Gentle pressure was applied on both sides of the incision to bring the left lobe of the liver into the wound. Custom 10mm-diameter circular-plate copper electrodes were affixed to calipers and connected to an ECM 830 Square Wave Electroporation System (BTX Harvard Apparatus, Holliston, MA). IRE of the liver was performed by gently holding the lateral half of the left lobe between the two electrodes, while avoiding contact of the electrodes with any other surface. The thickness of the liver lobe of each mouse was measured before IRE administration to determine the voltage required to deliver the prescribed electric field strength. Electrical pulses were applied using parameters of 750V/cm or 1500V/cm, 8 total 100μs square pulses, each pulse separated by 100ms. After IRE, the liver lobe was returned to the abdomen, and the abdominal incision closed by sutures in two layers. The mouse was then allowed to recover from anesthesia per standard peri-operative protocol.

Tissue Impedance Measurements.

Liver tissue impedance was measured using custom 10mm-diameter circular-plate copper electrodes connected to a 4294A Precision Impedance Analyzer (Agilent Technologies

Japan, Hyogo, Japan). The same 10mm circular electrodes were used for both IRE and for measuring impedance. In both cases, the surface of the electrodes encompassed the entire lateral half of the left lobe. Areas previously treated with IRE were identified anatomically. Impedance (Z) was measured over the entire range of electrical current frequencies from 40Hz to 20MHz. The magnitude of impedance at 10kHz ($|Z|_{10kHz}$) was representative of the magnitude of overall tissue impedance and determined over several biological replicates to show statistical significance. According to our previous experiment, the Cole model is valid to characterize the impedance spectrogram obtained from multi-frequency measurements before and after electroporation, and the value of impedance at zero frequency (resistance) can be computed as proportional to the impedance at 10kHz.[36] The resistance is scaled by the cell constant, *K*, defined as the ratio between the resistivity and the measured resistance, which depends on the sample geometry.[36] For each mouse at each timepoint, impedance was measured at the same location 3 times and values were averaged to represent the impedance of the tissue. All impedance measurements were performed *in vivo* while mice were under anesthesia. Impedance measurements 1, 3, and 7 days after IRE treatment were obtained by re-opening the previously made midline incision and delivering the left lobe out from the wound.

Histology.

Mouse liver was harvested and fixed in 10% formalin 1, 3, or 7 days after IRE treatment. Paraffin sectioning, hematoxylin and eosin (H&E), and Sirius Red staining were performed by the UCSF Liver Center Pathology Core using standard procedures.

Injury Area Analysis.

IRE injury area was quantified from H&E stained sections. Images were captured with a Zeiss Axiocam MRc5 color camera adapted to the photoport of a Zeiss AxioImager A1 upright microscope (Zeiss, Oberkochen, Germany) at the UCSF Biological Imaging Development Center (San Francisco, CA). Images were digitally acquired using Axiovision 4 imaging software (Zeiss). Injury area measurements were obtained by outlining the injured regions and determining the surface area using ImageJ software (Bethesda, MD).

Immunohistochemistry Staining.

Paraffin embedded samples were sectioned at 5μm and stained by HistoWiz Inc. (Brooklyn, NY) on a Bond Rx autostainer (Leica Biosystems, Buffalo Grove, IL) with enzyme treatment (1:1000) using standard protocols. Bond Polymer Refine Detection (Leica Biosystems) was used according to manufacturer's instructions. Antibodies used were Ly6G (RB6-8C5, 1:300; Abcam, Cambridge, MA), F4/80 (BM8, 1:200; eBioscience, San Diego, CA), and CD11b (EPR1344, 1:10000; Abcam). Sections were counterstained with hematoxylin, dehydrated and film coverslipped using a TissueTek-Prisma and Coverslipper (Sakura, Torrence, CA). Whole slide scanning was performed on an Aperio AT2 (Leica Biosystems) and analyzed using Aperio Image Scope software (Leica Biosystems).

Statistical Analysis.

Student's two-tailed t-tests and linear regression analyses were performed with GraphPad Prism version 7.01 (GraphPad, La Jolla, CA). Two-tailed p-values < 0.05 were considered statistically significant. Data were expressed as average ± standard error (SEM).

Results

Resistivity of fibrotic liver tissue is lower than that of control non-fibrotic liver.

The impedance measurements obtained from liver tissue *in vivo* while mice were under anesthesia differed significantly from values obtained from resected liver tissue *ex vivo* (data not shown). Therefore, all impedance and resistivity values reported in this study were obtained from *in vivo* measurements. DDC intoxication induces biliary fibrosis characterized by inflammatory infiltrates and deposition of aligned collagen fibers around the peri-portal areas (Figure 1A).[40] Average tissue resistivity of fibrotic liver from DDC-treated mice (1275±50 Ω·cm) was significantly lower than that of non-fibrotic liver from control mice (1593±51 Ω·cm, $p<0.001$) (Figure 1B). These results demonstrate that the electrical properties of fibrotic tissues are innately different from non-fibrotic tissues at baseline.

Resistivity of non-fibrotic liver decreases rapidly after IRE treatment, whereas the decrease in resistivity of fibrotic liver is slower.

We measured the change in resistivity of control and fibrotic liver minutes after IRE application at two electric field strengths. The electric field strength of 750V/cm is slightly above the lower threshold capable of inducing irreversible electroporation.[1] The electric field strength of 1500V/cm is commonly used in current clinical tissue ablation applications.[41] Electric fields were applied for 8 pulses at a pulse length of 100μs to avoid the electrolytic effects of applying a high number of pulses.[42] In control non-fibrotic liver, the resistivity of the tissue decreased significantly within minutes after IRE treatment at both 750V/cm and 1500V/cm, and stabilized after 10 minutes at −403±153 Ω·cm from baseline. Resistivity decreased more rapidly after 1500V/cm IRE than after 750V/cm IRE and stabilized at a lower value of −720±128 Ω·cm from baseline (Figure 2A). In contrast, the resistivity of fibrotic liver tissue increased slightly immediately after IRE treatment at 750V/cm and 1500V/cm (Figure 2B and 2C). Also in contrast to non-fibrotic liver, the resistivity of fibrotic liver tissue did not decrease significantly after IRE treatment at 1500V/cm (Figure 2C). Linear regression coefficients (i.e. slopes) of the two lines in Figure 2A were significantly different, indicating that the rate of resistivity decrease in response to 1500V/cm IRE was significantly faster compared to 750V/cm in non-fibrotic liver ($p<0.05$). Likewise, linear regression of the lines in Figure 2C showed that the rate of resistivity decrease in response to 1500V/cm IRE was significantly faster for control liver compared to fibrotic liver ($p<0.05$). These findings indicate that the immediate effects of IRE are different on non-fibrotic versus fibrotic liver tissue and that these differences are augmented at higher IRE electric field strengths.

Tissue resistivity of non-fibrotic liver recovers to baseline by 7 days after IRE treatment, but remains depressed in fibrotic liver.

To determine the effect of IRE treatment on tissue impedance on a longer time scale, we treated mouse livers with either 750V/cm or 1500V/cm IRE and then measured the impedance of the treated tissue 1, 3, or 7 days later. The tissue resistivity of fibrotic liver decreased significantly from baseline one day after 750V/cm IRE to 908±70 Ω·cm ($p<0.01$), whereas the resistivity of control liver remained relatively the same at 1523±135 Ω·cm (Figure 2D). In contrast, resistivity of both control and fibrotic liver dropped significantly one day after 1500V/cm IRE to 765±70 Ω·cm and 532±8 Ω·cm, respectively. Resistivity of fibrotic liver decreased to a lower level than that of control liver ($p<0.001$), and the reduction paralleled the lower baseline resistivity of fibrotic liver tissue (Figure 2E). Day 3 after IRE treatment marked a time of tissue resistivity recovery for both control and fibrotic liver treated with either electric field strength (Figure 2D and 2E). However, at day 7, the resistivity of control liver continued to increase (1823±238 Ω·cm for 750V/cm and 1337±69 Ω·cm for 1500V/cm), whereas the resistivity of fibrotic liver remained significantly depressed (1149±59 Ω·cm for 750V/cm, $p<0.05$ compared to control; 893±37 Ω·cm for 1500V/cm, $p<0.01$ compared to control) (Figure 2D and 2E). These data indicate that the response of non-fibrotic and fibrotic liver to IRE treatment is significantly different, especially at later timepoints.

To further illustrate the difference in response of control and fibrotic liver to IRE treatment, we determined the complex impedance of the tissues over the full range of electrical current frequencies. Measurements of impedance as a function of frequency from representative mice clearly demonstrated significant differences in response between control and fibrotic liver after 1500V/cm IRE treatment. Non-fibrotic liver showed significantly reduced impedance over the span of biologically relevant electrical frequencies at 1 and 3 days after 1500V/cm IRE and recovery of tissue impedance to baseline levels by day 7 (Figure 3). In contrast, at all timepoints after 1500V/cm IRE, fibrotic liver showed persistently reduced tissue impedance that did not recover at day 7. These differences in impedance profiles suggest that whereas non-fibrotic livers eventually regain their baseline electrical properties after IRE treatment, fibrotic livers do not.

Differences in tissue impedance correspond to differential effects on cell death and inflammation in control and fibrotic liver after IRE treatment.

Liver tissue histology was examined 1, 3, and 7 days after 750V/cm or 1500V/cm IRE treatment (Figure 4A). One day after IRE, control livers showed small homogenous areas of parenchymal cell death in response to 750V/cm (2.1±1.6mm^2) (Figure 4B) and larger areas of homogenous cell death in response to 1500V/cm (30.8±2.86mm^2) (Figure 4C). In contrast, fibrotic liver demonstrated patchy areas of cell death interspersed between peri-portal inflammation, ductular reaction, and fibrosis (Figure 4A). Larger zones of patchy parenchymal cell death developed in fibrotic liver after 1500V/cm compared to 750V/cm, but peri-portal areas of inflammation and fibrosis were largely spared. On day 3, areas of parenchymal cell death expanded in control livers treated with 750V/cm (17.0±2.2mm^2) and were significantly larger than the patchy areas of cell death in fibrotic livers treated with the same electric field strength (0.8±0.6mm^2, $p<0.001$) (Figure 4B). The area size of tissue

injury was comparable between control (38.0±6.0mm^2) and fibrotic livers (29.3±1.8mm^2) treated with 1500V/cm (Figure 4C). However, in control livers, there was very little inflammatory infiltration associated with areas of cell death, as opposed to fibrotic livers in which massive expansion of peri-portal inflammatory cells replaced the patchy areas of cell death (Figure 4A). On day 7 after 750V/cm ablation, consistent with previous reports,[3,6,27] control liver parenchyma repaired and regenerated itself without scarring. In fibrotic liver treated with 750V/cm, the parenchyma also returned to the pre-treatment baseline, showing peri-portal inflammation and no detectable areas of cell death (Figures 4A and 4B). After treatment of control liver with the higher electric field strength of 1500V/cm, a contracted area of inflammatory cellular infiltrate remained at the site of IRE treatment (4.4±2.4 mm^2), surrounded by normal-appearing liver tissue. In contrast, in the fibrotic liver after 1500V/cm IRE, the massive inflammatory infiltrate seen at day 3 persisted (30.0±0.4mm^2, $p<0.001$ compared to 1500V/cm control liver) and there were no signs of repopulation of the ablation zone with hepatocytes (Figures 4A and 4C). These histological findings demonstrate that the differences in tissue impedance after IRE treatment correlated with differing patterns of cell death and inflammatory response in non-fibrotic and fibrotic liver tissue.

To further characterize the inflammatory filtrate in control and fibrotic livers after IRE treatment, we performed immunohistochemistry for immune cell markers on day 3 post 1500V/cm IRE. Ly6G is a marker for neutrophils, F4/80 is a marker for Kupffer cells (resident liver macrophages), and CD11b is a marker for monocyte-derived macrophages.[43] There were very few Ly6G$^+$ or CD11b$^+$ cells in the parenchyma of non-fibrotic liver that did not receive IRE treatment. F4/80$^+$ cells were detected lining the sinusoids, consistent with the presence of Kupffer cells in normal liver homeostasis (Figure 5). In fibrotic liver without IRE treatment, there was Ly6G$^+$ and CD11b$^+$ cells present in the parenchyma and increased numbers of F4/80$^+$ cells around the peri-portal zones, consistent with ongoing inflammation in the setting of chronic liver injury. Non-fibrotic liver parenchyma treated with 1500V/cm IRE demonstrated greater numbers of Ly6G$^+$, F4/80$^+$, and CD11b$^+$ cells compared to uninjured non-fibrotic liver, and these cells were mostly localized to peri-portal areas. In contrast, fibrotic liver treated with 1500V/cm IRE showed disseminated Ly6G$^+$ cells, massive infiltration of F4/80$^+$ cell, and large clusters of CD11b$^+$ cells throughout the injured tissue. These finding suggest that there is greater recruitment and activation of neutrophils, Kupffer cell, and monocyte-derived macrophages in fibrotic liver as compared to non-fibrotic liver after treatment with 1500V/cm IRE.

Discussion

Our results show there are important differences in the electrical properties of non-fibrotic and fibrotic liver tissues, and the presence of fibrosis modulates tissue response to IRE treatment. First of all, the baseline resistivity of fibrotic liver was lower than that of non-fibrotic liver. Although electrical current may flow more easily through fibrotic liver, the rate of resistivity decrease immediately after IRE treatment was attenuated in fibrotic liver compared to non-fibrotic control. At later timepoints, the resistivity of fibrotic liver was significantly lower than that of the control liver at days 1 and 7 after IRE treatment, whereas control and fibrotic liver resistivities were comparable on day 3 post-IRE. Importantly, 7 days after IRE treatment, the impedance profile of control liver returned to near pre-

treatment baseline, but the impedance of fibrotic liver remained significantly depressed. Recovery of tissue impedance in control liver correlated with repopulation of the ablated liver parenchyma with hepatocytes, without formation of scar. Reduced tissue impedance in fibrotic liver corresponded with persistent inflammatory infiltrates in the ablated tissue.

The effect of fibrosis on the conductivity of tissues is not well understood. In computational models of cardiac fibrosis, fibrotic septae have been incorporated as non-conductive bands that either slow overall conduction or behave as decoupling elements that promote re-entrant arrhythmias.[28,44] Our results suggest that fibrotic tissues have lower resistivities compared to controls and therefore allow easier passage of electrical current. It is possible that fibrotic bands distort tissue architecture in a way that creates “short-circuits” through the parenchyma, leading to lower resistivity in fibrotic liver. If so, IRE applied at a uniform voltage may have heterogeneous effects within a fibrotic tissue volume, which has important implications for the treatment of highly fibrotic tumors like pancreas adenocarcinoma.

The effects of IRE on the resistivities of control and fibrotic livers were different and depended on the electric field strength and timepoint after treatment. In general, we saw similar trends in tissue response to 750V/cm (electric field strength near the lower threshold of inducing IRE) and 1500V/cm (electric field strength typically used in clinical tumor ablations). Differences demonstrated between control and fibrotic livers after 750V/cm IRE were augmented after 1500V/cm IRE. Changes in resistivity at various timepoints after IRE likely reflect different underlying biological processes. Minutes after IRE treatment, decreases in tissue impedance are dominated by increased current flow as a result of the permeabilization of cell membranes.[36] Compared to resistivity in control liver, fibrotic liver resistivity decreased significantly more slowly right after IRE treatment, suggesting that the rate of cell membrane permeabilization may be attenuated in fibrotic tissues.

Previous studies indicate that IRE-induced cell death manifests by 6 hours after treatment and continues to evolve for up to 3 days, at which point tissue repair begins. Repopulation of the ablated tissue with new parenchymal cells may be complete by days 7-14. [3,6,10,27] In our study, both non-fibrotic and fibrotic liver tissues demonstrated cell death at days 1 and 3 after IRE. However, in contrast to the homogenous ablation zone in the control liver, fibrotic liver demonstrated patchy areas of hepatocyte cell death with sparing of the inflammatory infiltrates around the portal tracts. This is consistent with the idea that IRE may induce “short-circuits” within fibrotic tissues, resulting in heterogeneous patterns of cell death. In addition, susceptibility to electroporation is dependent on cell size and morphology, and smaller cells require higher voltages.[29-32] Therefore, the sparing of inflammatory infiltrates and areas of fibrosis may also be because immune cells and myofibroblasts are significantly smaller than hepatocytes. Importantly, unlike in non-fibrotic liver, 1500V/cm IRE induced severe and persistent inflammation at the site of ablation in fibrotic liver. Whereas control livers showed repopulation of the ablation site with hepatocytes, without formation of scar, fibrotic livers demonstrated massive ongoing inflammatory infiltrates at 7 days post-IRE. Repopulation of the ablation zone with hepatocytes in control livers correlated with recovery of tissue impedance back to pre-IRE levels. Persistent inflammation in fibrotic livers correlated with persistently reduced tissue impedance measured through a range of frequencies. These results suggest that in fibrotic tissues, IRE administered at the commonly

used electric field strength (i.e. 1500V/cm) does not kill fibrosis-associated inflammatory infiltrates and may additionally promote the inflammatory process. Furthermore, our findings suggest that the regenerative mechanisms induced in non-fibrotic tissues after IRE may be inhibited or dysregulated in fibrotic tissues.

The clinical implications of our findings are significant, because we show that the effect of IRE is modulated by the tissue microenvironment. Tumor microenvironments have important roles in modulating tumor aggressiveness, metastases, and response to treatment.[45] We show that IRE induces a different pattern of tissue ablation and inflammatory response activation in non-fibrotic versus fibrotic liver parenchyma. These differences may impact the way tumors that arise in non-fibrotic liver (e.g. colorectal metastases) respond to IRE compared to tumors that arise in fibrotic liver (e.g. hepatocellular carcinoma), especially in the setting of combination immunotherapy. As such, an interesting and important area of future investigation would be to determine whether the amplified IRE-induced inflammatory reaction in fibrotic tissues promotes or inhibits tumor progression. In addition, our findings suggest that IRE-induced “scarless regeneration” may be inhibited or dysregulated in fibrotic tissues, posing a challenge to using IRE to facilitate regenerative surgery in failing organs that are fibrotic. However, since we show that IRE has distinct effects on inflammatory infiltrates and areas of fibrosis, our results also open new possibilities of using IRE to re-educate the stroma and induce remodeling of the tissue microenvironment.

Acknowledgments

We thank Ms. Pamela Derish for editorial assistance.

Funding

This work was supported by the National Institutes of Health [R21-EB024135], [P30-DK026743], and the Open Philanthropy Project [Transformative Research Award].

References

1. Davalos RV, Mir IL, and Rubinsky B. Tissue ablation with irreversible electroporation. Ann Biomed Eng. 2005; 33: 223–31. [PubMed: 15771276]
2. Maor E, Ivorra A, Leor J, and Rubinsky B. The effect of irreversible electroporation on blood vessels. Technol Cancer Res Treat. 2007; 6: 307–12. [PubMed: 17668938]
3. Rubinsky B, Onik G, and Mikus P. Irreversible electroporation: a new ablation modality--clinical implications. Technol Cancer Res Treat. 2007; 6: 37–48. [PubMed: 17241099]
4. Phillips MA, Narayan R, Padath T, and Rubinsky B. Irreversible electroporation on the small intestine. Br J Cancer. 2012; 106: 490–5. doi:10.1038/bjc.2011.582. [PubMed: 22223084]
5. Golberg A, Broelsch GF, Bohr S, Mihm MC Jr., Austen WG Jr., Albadawi H, et al. Non-thermal, pulsed electric field cell ablation: A novel tool for regenerative medicine and scarless skin regeneration. Technology (Singap World Sci). 2013; 1: 1–8. doi:10.1142/S233954781320001X. [PubMed: 24999487]
6. Golberg A, Bruinsma BG, Jaramillo M, Yarmush ML, and Uygun BE. Rat liver regeneration following ablation with irreversible electroporation. PeerJ. 2016; 4: e1571. doi:10.7717/peerj.1571. [PubMed: 26819842]
7. Guo Y, Zhang Y, Klein R, Nijm GM, Sahakian AV, Omary RA, et al. Irreversible electroporation therapy in the liver: longitudinal efficacy studies in a rat model of hepatocellular carcinoma. Cancer Res. 2010; 70: 1555–63. doi:10.1158/0008-5472.CAN-09-3067. [PubMed: 20124486]

8. Lee EW, Chen C, Prieto VE, Dry SM, Loh CT, and Kee ST. Advanced hepatic ablation technique for creating complete cell death: irreversible electroporation. Radiology. 2010; 255: 426–33. doi:10.1148/radiol.10090337. [PubMed: 20413755]
9. Kim HB, Sung CK, Baik KY, Moon KW, Kim HS, Yi JH, et al. Changes of apoptosis in tumor tissues with time after irreversible electroporation. Biochem Biophys Res Commun. 2013; 435: 651–6. doi:10.1016/j.bbrc.2013.05.039. [PubMed: 23688425]
10. Zhang Y, Lyu C, Liu Y, Lv Y, Chang TT, and Rubinsky B. Molecular and histological study on the effects of non-thermal irreversible electroporation on the liver. Biochem Biophys Res Commun. 2018; 500: 665–70. doi:10.1016/j.bbrc.2018.04.132. [PubMed: 29678581]
11. Bulvik BE, Rosenblum N, Gourevich S, Ahmed M, Andriyanov AV, Galun E, et al. Irreversible electroporation versus radiofrequency ablation: A comparison of local and systemic effects in a small animal model. Radiology. 2016.
12. Martin RC 2nd, Kwon D, Chalikonda S, Sellers M, Kotz E, Scoggins C, et al. Treatment of 200 locally advanced (stage III) pancreatic adenocarcinoma patients with irreversible electroporation: safety and efficacy. Ann Surg. 2015; 262: 486–94; discussion 92-4. doi:10.1097/SLA.0000000000001441. [PubMed: 26258317]
13. Kluger MD, Epelboym I, Schrope BA, Mahendraraj K, Hecht EM, Susman J, et al. Single-Institution Experience with Irreversible Electroporation for T4 Pancreatic Cancer: First 50 Patients. Ann Surg Oncol. 2016; 23: 1736–43. doi:10.1245/s10434-015-5034-x. [PubMed: 26714959]
14. Scheffer HJ, Vroomen LG, de Jong MC, Melenhorst MC, Zonderhuis BM, Daams F, et al. Ablation of Locally Advanced Pancreatic Cancer with Percutaneous Irreversible Electroporation: Results of the Phase I/II PANFIRE Study. Radiology. 2017; 282: 585–97. doi:10.1148/radiol.2016152835. [PubMed: 27604035]
15. Vogel JA, Rombouts SJ, de Rooij T, van Delden OM, Dijkgraaf MG, van Gulik TM, et al. Induction Chemotherapy Followed by Resection or Irreversible Electroporation in Locally Advanced Pancreatic Cancer (IMPALA): A Prospective Cohort Study. Ann Surg Oncol. 2017; 24: 2734–43. doi:10.1245/s10434-017-5900-9. [PubMed: 28560601]
16. Scheffer HJ, Vroomen LG, Nielsen K, van Tilborg AA, Comans EF, van Kuijk C, et al. Colorectal liver metastatic disease: efficacy of irreversible electroporation--a single-arm phase II clinical trial (COLDFIRE-2 trial). BMC Cancer. 2015; 15: 772. doi:10.1186/s12885-015-1736-5. [PubMed: 26497813]
17. Niessen C, Thumann S, Beyer L, Pregler B, Kramer J, Lang S, et al. Percutaneous Irreversible Electroporation: Long-term survival analysis of 71 patients with inoperable malignant hepatic tumors. Sci Rep. 2017; 7: 43687. doi:10.1038/srep43687. [PubMed: 28266600]
18. Sutter O, Calvo J, N'Kontchou G, Nault JC, Ourabia R, Nahon P, et al. Safety and Efficacy of Irreversible Electroporation for the Treatment of Hepatocellular Carcinoma Not Amenable to Thermal Ablation Techniques: A Retrospective Single-Center Case Series. Radiology. 2017; 284: 877–86. doi:10.1148/radiol.2017161413. [PubMed: 28453431]
19. Fruhling P, Nilsson A, Duraj F, Haglund U, and Noren A. Single-center nonrandomized clinical trial to assess the safety and efficacy of irreversible electroporation (IRE) ablation of liver tumors in humans: Short to mid-term results. Eur J Surg Oncol. 2017; 43: 751–7. doi:10.1016/j.ejso.2016.12.004. [PubMed: 28109674]
20. Coelen RJS, Vogel JA, Vroomen L, Roos E, Busch ORC, van Delden OM, et al. Ablation with irreversible electroporation in patients with advanced perihilar cholangiocarcinoma (ALPACA): a multicentre phase I/II feasibility study protocol. BMJ Open. 2017; 7: e015810. doi:10.1136/bmjopen-2016-015810.
21. Zimmerman A, Grand D, and Charpentier KP. Irreversible electroporation of hepatocellular carcinoma: patient selection and perspectives. J Hepatocell Carcinoma. 2017; 4: 49–58. doi:10.2147/JHC.S129063. [PubMed: 28331845]
22. Lin M, Liang S, Wang X, Liang Y, Zhang M, Chen J, et al. Percutaneous irreversible electroporation combined with allogeneic natural killer cell immunotherapy for patients with unresectable (stage III/IV) pancreatic cancer: a promising treatment. J Cancer Res Clin Oncol. 2017; 143: 2607–18. doi:10.1007/s00432-017-2513-4. [PubMed: 28871458]

23. Alnaggar M, Lin M, Mesmar A, Liang S, Qaid A, Xu K, et al. Allogenic natural killer cell immunotherapy combined with irreversible electroporation for stage IV hepatocellular carcinoma: survival outcome. Cell Physiol Biochem. 2018; 48: 1882–93. doi: 10.1159/000492509. [PubMed: 30092590]
24. Phillips M, Maor E, and Rubinsky B. Nonthermal irreversible electroporation for tissue decellularization. J Biomech Eng. 2010; 132: 091003. doi:10.1115/1.4001882. [PubMed: 20815637]
25. Phillips M, Maor E, and Rubinsky B. Principles of tissue engineering with nonthermal irreversible electroporation. Journal of Heat Transfer. 2011; 133: 0110041–8.
26. Phillips MA, Maor E, Rubinsky B, and Lavee J. Extracellular matrix material created using non-thermal irreversible electroporation. . US Patent 08835166, Sep 16 2014. The Regents of the University of California 2014.
27. Chang TT, Zhou VX, and Rubinsky B. Using non-thermal irreversible electroporation to create an in vivo niche for exogenous cell engraftment. BioTechniques. 2017; 62: 229–31. doi:10.2144/000114547. [PubMed: 28528576]
28. Gokhale TA, Medvescek E, and Henriquez CS. Modeling dynamics in diseased cardiac tissue: Impact of model choice. Chaos. 2017; 27: 093909. doi:10.1063/1.4999605. [PubMed: 28964161]
29. Kekez MM, Savic P, and Johnson BF. Contribution to the biophysics of the lethal effects of electric field on microorganisms. Biochim Biophys Acta. 1996; 1278: 79–88. [PubMed: 8611611]
30. Agarwal A, Zudans I, Weber EA, Olofsson J, Orwar O, and Weber SG. Effect of cell size and shape on single-cell electroporation. Anal Chem. 2007; 79: 3589–96. doi:10.1021/ac062049e. [PubMed: 17444611]
31. Kaner A, Braslavsky I, and Rubinsky B. Model of pore formation in a single cell in a flow-through channel with micro-electrodes. Biomed Microdevices. 2014; 16: 181–9. doi:10.1007/s10544-013-9820-6. [PubMed: 24150603]
32. Ivey JW, Latouche EL, Richards ML, Lesser GJ, Debinski W, Davalos RV, et al. Enhancing Irreversible Electroporation by Manipulating Cellular Biophysics with a Molecular Adjuvant. Biophys J. 2017; 113: 472–80. doi:10.1016/j.bpj.2017.06.014. [PubMed: 28746857]
33. Vidal-Vanaclocha F The prometastatic microenvironment of the liver. Cancer Microenviron. 2008; 1: 113–29. doi:10.1007/s12307-008-0011-6. [PubMed: 19308690]
34. Augustin G, Bruketa T, Korolija D, and Milosevic M. Lower incidence of hepatic metastases of colorectal cancer in patients with chronic liver diseases: meta-analysis. Hepatogastroenterology. 2013; 60: 1164–8. doi:10.5754/hge11561. [PubMed: 23803379]
35. Ramachandran P, and Iredale JP. Reversibility of liver fibrosis. Ann Hepatol. 2009; 8: 283–91. [PubMed: 20009126]
36. Ivorra A, and Rubinsky B. In vivo electrical impedance measurements during and after electroporation of rat liver. Bioelectrochemistry. 2007; 70: 287–95. doi: 10.1016/j.bioelechem.2006.10.005. [PubMed: 17140860]
37. Bonakdar M, Latouche EL, Mahajan RL, and Davalos RV. The feasibility of a smart surgical probe for verification of IRE treatments using electrical impedance spectroscopy. IEEE Trans Biomed Eng. 2015; 62: 2674–84. doi:10.1109/TBME.2015.2441636. [PubMed: 26057529]
38. Kranjc M, Kranjc S, Bajd F, Sersa G, Sersa I, and Miklavcic D. Predicting irreversible electroporation-induced tissue damage by means of magnetic resonance electrical impedance tomography. Sci Rep. 2017; 7: 10323. doi:10.1038/s41598-017-10846-5. [PubMed: 28871138]
39. Hanada S, Snider NT, Brunt EM, Hollenberg PF, and Omary MB. Gender dimorphic formation of mouse Mallory-Denk bodies and the role of xenobiotic metabolism and oxidative stress. Gastroenterology. 2010; 138: 1607–17. doi:10.1053/j.gastro.2009.12.055. [PubMed: 20064513]
40. Fickert P, Stoger U, Fuchsbichler A, Moustafa T, Marschall HU, Weiglein AH, et al. A new xenobiotic-induced mouse model of sclerosing cholangitis and biliary fibrosis. Am J Pathol. 2007; 171: 525–36. doi:10.2353/ajpath.2007.061133. [PubMed: 17600122]
41. Martin RC 2nd, Durham AN, Besselink MG, Iannitti D, Weiss MJ, Wolfgang CL, et al. Irreversible electroporation in locally advanced pancreatic cancer: A call for standardization of energy delivery. J Surg Oncol. 2016; 114: 865–71. doi:10.1002/jso.24404. [PubMed: 27546233]

42. Rubinsky L, Guenther E, Mikus P, Stehling M, and Rubinsky B. Electrolytic effects during tissue ablation by electroporation. Technol Cancer Res Treat. 2016; 15: NP95–NP103. doi: 10.1177/1533034615601549.

43. Krenkel O, and Tacke F. Liver macrophages in tissue homeostasis and disease. Nat Rev Immunol. 2017; 17: 306–21. doi:10.1038/nri.2017.11. [PubMed: 28317925]

44. de Jong S, van Veen TA, van Rijen HV, and de Bakker JM. Fibrosis and cardiac arrhythmias. J Cardiovasc Pharmacol. 2011; 57: 630–8. doi:10.1097/FJC.0b013e318207a35f. [PubMed: 21150449]

45. Quail DF, and Joyce JA. Microenvironmental regulation of tumor progression and metastasis. Nat Med. 2013; 19: 1423–37. doi:10.1038/nm.3394. [PubMed: 24202395]

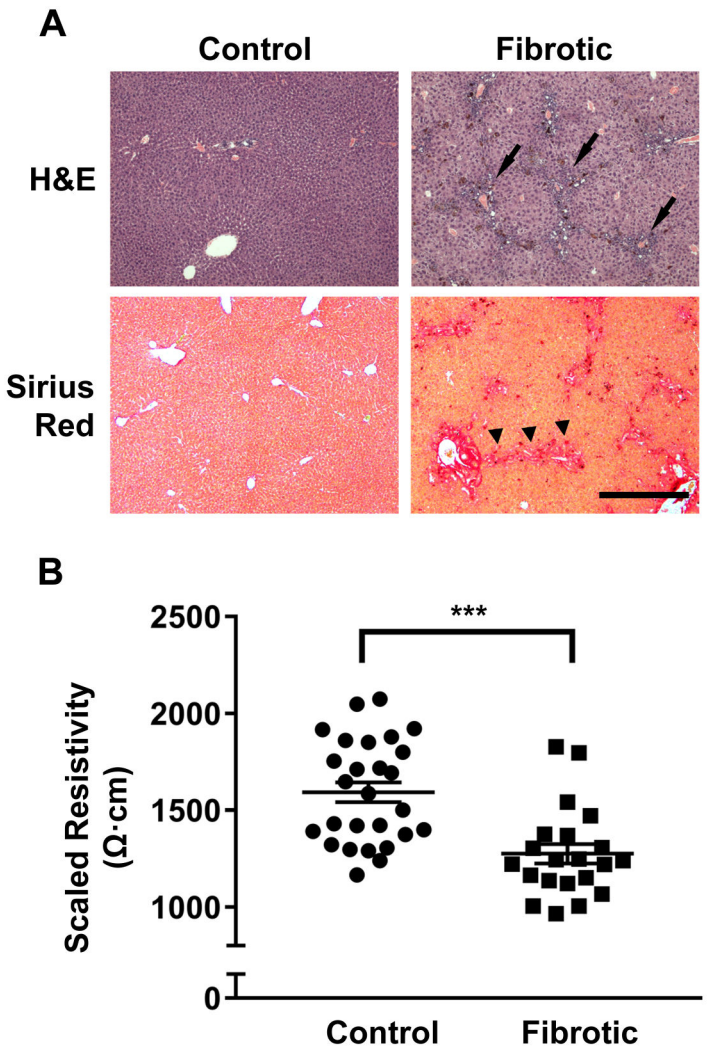

Figure 1. Fibrotic liver tissue with peri-portal inflammation and collagen deposition demonstrates lower electrical resistivity than non-fibrotic liver tissue.

(A) Hematoxylin and eosin (H&E) and Sirius Red histologic staining of control non-fibrotic and fibrotic liver tissue. After 4 weeks of 0.1% DDC diet, mice develop peri-portal inflammatory infiltrates (arrows) and collagen deposition with portal-portal bridging fibrosis (arrowheads). Magnification 4x. Scale bar = 500μm for all images. (B) Baseline resistivity is significantly lower in fibrotic liver compared to control non-fibrotic liver. Liver tissue resistivity at 10kHz was determined in control mice (n=27) and mice fed a 0.1% DDC diet for 4 weeks (n=21). ***p<0.001 by Student's t-test.

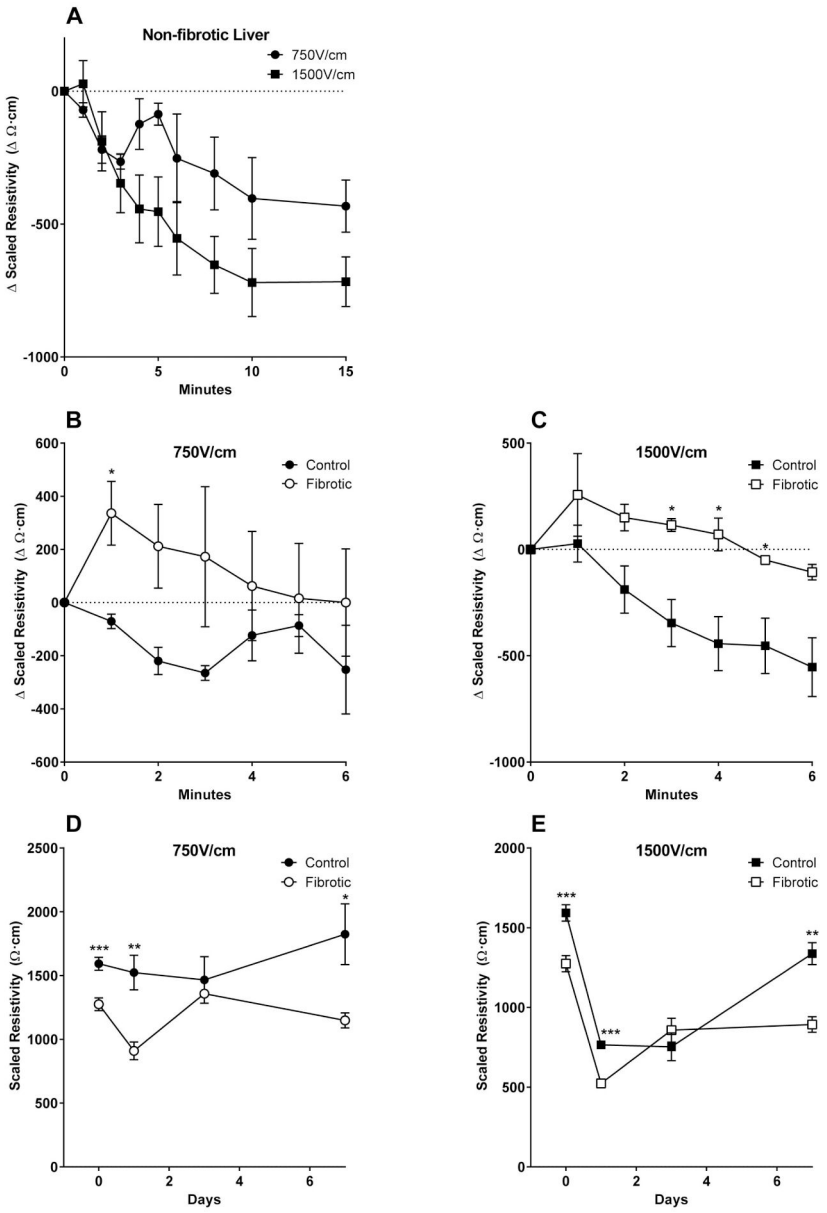

Figure 2. Liver tissue resistivity after IRE treatment is modulated by the electric field strength and presence of fibrosis.

The change in tissue resistivity at 10kHz (Δ Ω·cm) was determined by subtracting the pre-IRE baseline resistivity from the resistivity determined at 1, 2, or 5 minute intervals post-IRE for up to 15 minutes (A-C) or absolute resistivity (Ω·cm) was determined at 10kHz at baseline prior to IRE (day 0) and at 1, 3, or 7 days after IRE treatment (D-E). (A) Early response of control non-fibrotic liver after 750V/cm or 1500V/cm IRE treatment. (B) Early response of control versus fibrotic liver tissue after 750V/cm IRE. (C) Early response of control versus fibrotic liver tissue after 1500V/cm IRE. (D) Later response of control versus fibrotic liver tissue after 750V/cm IRE. (E) Later response of control versus fibrotic liver tissue after 1500V/cm IRE. Day 0 resistivity data shown in D-E are the baseline resistivity data presented in Figure 1. All other resistivity data represent measurement in 3-5

independent animals in each group of mice at each timepoint (n=3-5). Regression coefficients (i.e. slopes that represent the rate of resistivity decrease) comparing 750V/cm versus 1500V/cm in non-fibrotic liver (A) and control versus fibrotic liver after 1500V/cm treatment (C) are significantly different ($p<0.05$). Asterisks show the timepoints in which resistivity was significantly different between control and fibrotic liver (B-E). *$p<0.05$, **$p<0.01$, ***$p<0.001$ by Student's t-test. Error bars represent SEM.

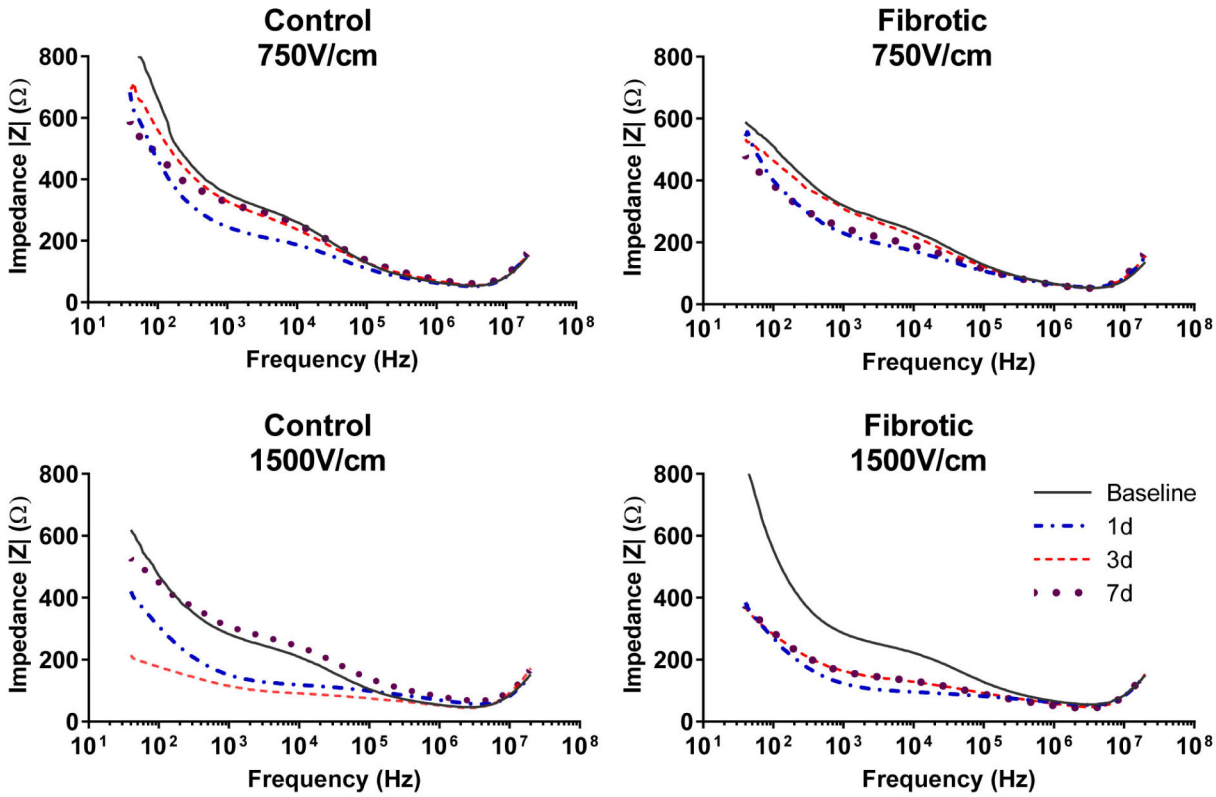

Figure 3. Impedance of non-fibrotic liver returns to baseline by day 7 after IRE treatment, whereas impedance of fibrotic liver remains significantly depressed.

Lines represent the magnitude of tissue impedance (|Z|) in the livers of representative mice in each group as determined through the entire range of electrical frequencies. By day 7 after IRE, the impedance of control non-fibrotic liver returns to pre-treatment baselines. In contrast, the impedance of fibrotic liver after 1500V/cm IRE remains significantly reduced.

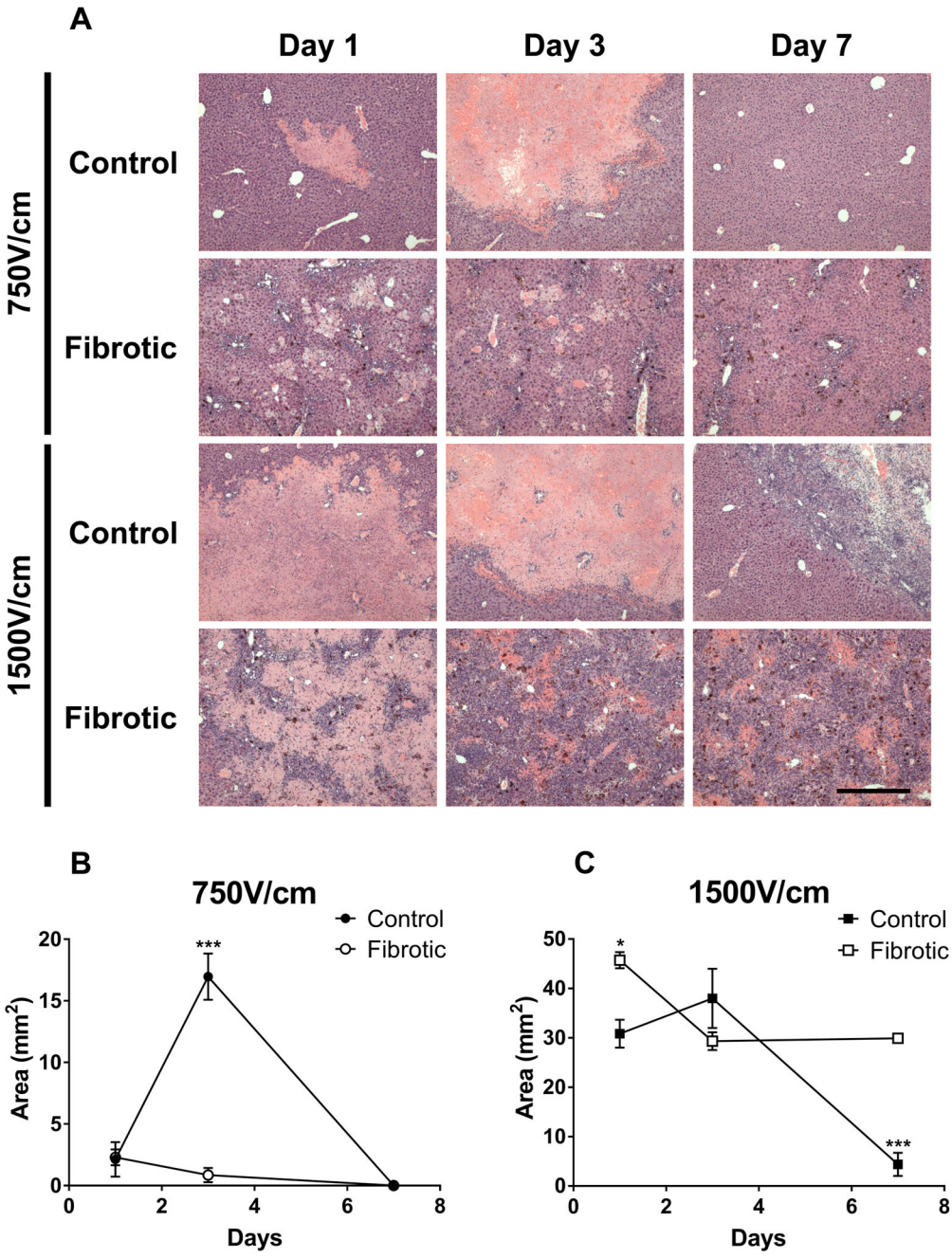

Figure 4. Patterns of cell death and inflammation after IRE treatment are different in fibrotic liver compared to control liver.

(A) Histology of control and fibrotic liver was examined by H&E staining on days 1, 3, and 7 after 750V/cm or 1500V/cm IRE treatment. Histology shows recovery of both control and fibrotic liver to baseline tissue architecture by 7 days after 750V/cm IRE. Control liver shows partial recovery of normal liver parenchyma at 7 days after 1500V/cm IRE. In contrast, fibrotic liver demonstrates persistent and severe inflammatory infiltrates at 7 days after 1500V/cm IRE. Magnification 4x. Scale bar = 500μm for all images. (B) Injury area size after 750V/cm IRE treatment in control and fibrotic liver. (C) Injury area size after

1500V/cm IRE treatment in control and fibrotic liver. Measured injury areas include areas of cell death and associated inflammatory infiltration. Histology images (A) are representative of 3-5 mice at each timepoint for each group (n=3-5), with the exception of “day 1-fibrotic liver-1500V/cm” for which n=2. Injury area data (B-C) represent the average injury area for each group at each timepoint, with error bars showing SEM. Asterisks show the timepoints in which injury area was significantly different between control and fibrotic liver. *$p<0.05$, ***$p<0.001$ by Student’s t-test.

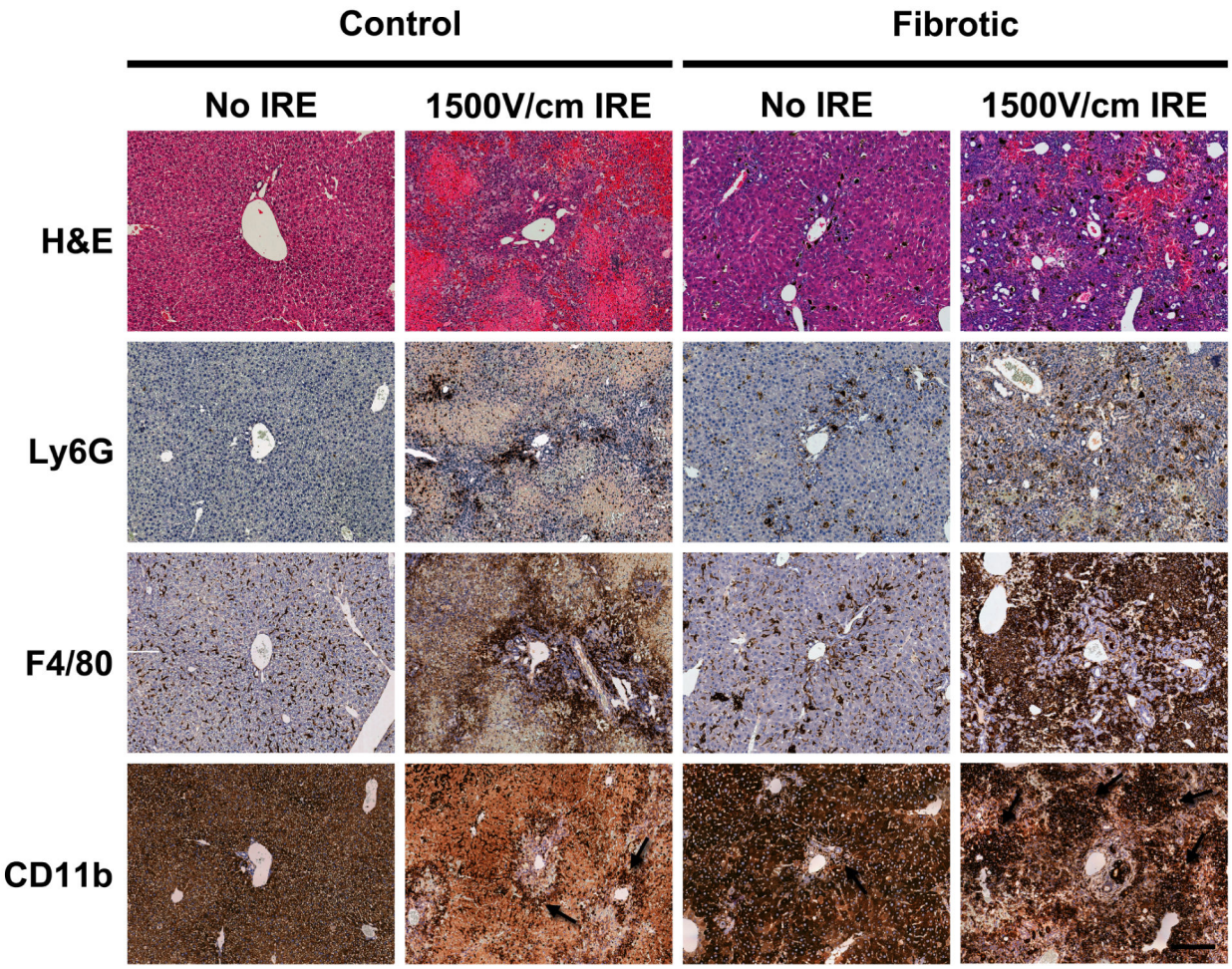

Figure 5. There is greater recruitment and activation of neutrophils, Kupffer cells, and monocyte-derived macrophages in fibrotic liver treated with IRE as compared to control non-fibrotic liver.

Immune cell infiltrates were characterized by staining for Ly6G (neutrophils), F4/80 (Kupffer cells - resident liver macrophages), and CD11b (monocyte-derived macrophages.) Control and fibrotic livers were analyzed 3 days after 1500V/cm IRE treatment. Liver parenchyma treated with IRE (1500V/cm IRE) and adjacent uninjured parenchyma (No IRE) were examined. Dark brown cells represent positive antibody staining. Uninjured liver parenchyma demonstrated high background staining to the CD11b antibody; arrows point to dark brown cells with positive CD11b antibody staining in the bottom row of images. Magnification 12x. Scale bar = 200μm for all images.